

# THE LIKELY *FERMI* DETECTION OF GRO J1008–57: HINT FOR $\gamma$ -RAY PRODUCTION IN NEUTRON-STAR X-RAY BINARIES

YI XING & ZHONGXIANG WANG

Key Laboratory for Research in Galaxies and Cosmology, Shanghai Astronomical Observatory, Chinese Academy of Sciences, 80 Nandan Road, Shanghai 200030, China

*Draft version February 5, 2019*

## ABSTRACT

In our search for  $\gamma$ -ray emission from Be X-ray binaries from analysis of the data obtained with the Large Area Telescope (LAT) on board the *Fermi Gamma-Ray Space Telescope*, we find likely detection of GRO J1008–57. The binary has an orbital period of 249.48 days, and it is only significantly detected in its orbital phase 0.8–0.9 ( $> 4\sigma$ ) and may be marginally detected in orbital phase 0.5–0.7. Further light curve analysis indicates that the former detection is probably largely due to an emitting event in one orbital cycle around year 2012–2013, following a giant outburst of the source. The combination of the stellar rotation, magnetic field, and mass accretion of the neutron star (a transient X-ray pulsar with a spin period of 93.5 s) makes GRO J1008–57 a system in which its propeller phase can be switched on in the quiescent state when its X-ray luminosity is lower than  $\sim 10^{34}$  erg s<sup>−1</sup>. Considering these features, we suggest that occasional  $\gamma$ -ray emitting events occur in GRO J1008–57. Particularly after a giant outburst, which probably would exhaust large amount of disk matter and induce the propeller phase in the following orbital phase, then similar to the transitional pulsar binaries (with PSR J1023+0038 as a prototype), the neutron star’s propeller processes or even its partial pulsar wind would result in the observed  $\gamma$ -ray emission. If this is confirmed, GRO J1008–57 may represent a type of transient  $\gamma$ -ray sources among neutron-star XRBs.

*Subject headings:* gamma rays: stars – stars: neutron – pulsars: individual (GRO J1008–57)

## 1. INTRODUCTION

X-ray binaries (XRBs) contain a compact primary, either a black hole or a neutron star, and when the companion is an early-type (O/B) massive star, such XRBs are classified as high-mass X-ray binaries (HMXBs). Generally the compact star in an HMXB system accretes from matter carried in the stellar wind of the companion and in most cases the accretion rates are low (e.g., Davidson & Ostriker 1973; Lamers et al. 1976; Walter et al. 2015). High X-ray luminosities ( $10^{35}$ – $10^{40}$  erg s<sup>−1</sup>) can be observed when the compact star is interacting with the dense part of the stellar wind of a Be star companion. Be XRBs account for a majority of the known HMXBs ( $\sim 50\%$ ; Walter et al. 2015), in most of which the compact stars are magnetized neutron stars (Liu et al. 2006; Lutovinov & Tsygankov 2009).

There are three Be XRBs, PSR B1259–63/LS 2883 (Aharonian et al. 2009; Tam et al. 2011; Abdo et al. 2011), LS I +61°303 (Abdo et al. 2009; Hadasch et al. 2012), and HESS 0632+057 (Hinton et al. 2009; Bongiorno et al. 2011; Li et al. 2017). They have been seen to emit photons in GeV–TeV  $\gamma$ -ray band. They are also classified as  $\gamma$ -ray binaries as their spectral energy distributions peak in  $\gamma$ -ray energies (Dubus 2013). PSR B1259–63/LS 2883 is the only  $\gamma$ -ray binary with a known  $\sim 47.8$  ms radio pulsar (Johnston et al. 1992). The pulsar moves around the Be-type companion with a long orbital period of  $\sim 3.4$  years and a high eccentricity of 0.87 (Johnston et al. 1994), and during the periastron passage a strong flare particularly at high-energies of X-ray to  $\gamma$ -ray is induced due to the close interaction between the winds of the two stars (e.g., Chernyakova et al. 2014; Tam et al. 2015; see also Xing et al. 2016). Recently an-

other pulsar system PSR 2032+4127/MT91 213 has also been found to be a candidate  $\gamma$ -ray binary system with a pulsar moving around a Be-type companion in a  $\sim 50$  year long orbit (Lyne et al. 2015; Ho et al. 2017).

Currently there are only five confirmed  $\gamma$ -ray binaries in the Galaxy (including the above three). While the limited number may provide constraints on binary evolution and high-energy physical processes (e.g., Meurs & van den Heuvel 1989; Dubus 2013), searches for more members of this class or related sources with  $\gamma$ -ray emission will help improve our understanding. Be XRBs are good candidates for such searches because of the existence of the circumstellar disks, providing an environment for different possible interactions with the neutron star primaries. For example, Romero et al. (2001) has reported the likely detection of the variable  $\gamma$ -ray emission from a Be XRB system A 0535+26. The  $\gamma$ -ray emission was suggested to originate in hadronic processes, in which hadrons accelerated from the magnetosphere of the neutron star could impact the surrounding accretion disk and produce  $\gamma$ -ray photons via the neutral pion decay process (e.g., Cheng & Ruderman 1991). However, no  $\gamma$ -ray emission from this source was detected during a giant X-ray outburst (Acciari et al. 2011). Motivated by these and taking advantage of the all-sky monitoring capability of the Large Area Telescope (LAT) onboard the *Fermi Gamma-ray Space Telescope* (*Fermi*), we conducted search for  $\gamma$ -ray emission from Be XRBs. The targets were selected from those given in Walter et al. (2015). Considering the X-ray and  $\gamma$ -ray emission from this type of sources are generally orbitally modulated, we only included the sources with known orbital parameters, allowing to conduct orbital-phase resolved search. Such search may be more sensitive due to orbitally-dependent

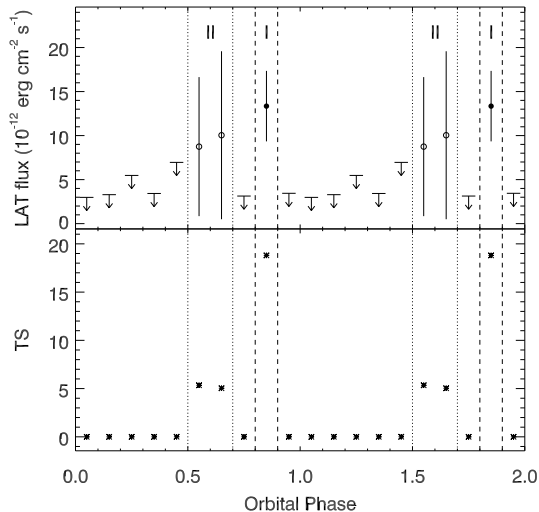


FIG. 1.— Orbital light curve and TS curve (0.3–500 GeV) for GRO J1008–57 obtained from *Fermi* LAT data. Flux points with TS greater than 9 and 5 are plotted with solid and open circles respectively, and the 95% upper limits are plotted otherwise.

physical processes (see, e.g., Xing et al. 2016).

In our search, likely detections of GRO J1008–57 in its certain orbital phase ranges were found. This Be XRB, discovered in 1993 (Stollberg et al. 1993), contains a spin period  $P = 93.5$  s transient X-ray pulsar, whose pulsed emission was detectable during the source’s X-ray outbursts (e.g., Coe et al. 2007; Kühnel et al. 2013). The binary has an orbit with a period of 249.48 days and an eccentricity of 0.68, determined from long-term timing of the pulsar’s pulsed emission (Coe et al. 2007; Kühnel et al. 2013). The magnetic field of the pulsar is known to be the highest among the Be XRBs, likely as high as  $\sim 8 \times 10^{12}$  G given the suggested cyclotron line at  $\sim 88$  keV (Shrader et al. 1999). GRO J1008–57 exhibits type-I X-ray outbursts periodically at each periastron passage (e.g., Tsygankov et al. 2017), due to the interaction between the neutron star and the circumstellar disk around the Be companion (e.g., Reig 2011), and occasionally type-II outbursts. The latter type of the outbursts in Be XRBs, which are much stronger than type-I, is believed to cause major changes in the structure of the circumstellar disk, sometimes even leading to the disappearance of the disk (Reig 2011).

In this paper, we report our results obtained for GRO J1008–57 from our analysis of the *Fermi* LAT data.

## 2. *Fermi* LAT DATA ANALYSIS AND RESULTS

### 2.1. LAT Data and Source Model

LAT scans the whole sky every three hours in the energy band of 0.1–500 GeV (Atwood et al. 2009). In the analysis, we selected LAT events from the *Fermi* Pass 8 database in the time period from 2008-08-04 15:43:36 (UTC) to 2017-10-19 00:56:35 (UTC). For GRO J1008–57, a  $20^\circ \times 20^\circ$  region centered at its position was selected. We followed the recommendations of the LAT team<sup>1</sup> by including the events with zenith angles less than 90 degrees (to prevent the Earth’s limb contamination) and excluding the events with quality flags of ‘bad’.

<sup>1</sup> <http://fermi.gsfc.nasa.gov/ssc/data/analysis/scitools/>

All sources within a 20 degree region centered at the target in the *Fermi* LAT 4-year catalog (Acero et al. 2015) were included to make the source model. Spectral forms of these sources are provided in the catalog. Spectral parameters of the sources within 5 degrees from the target were set as free parameters, and parameters of other sources were fixed at their catalog values. GRO J1008–57 was included in the source model as a point source with power-law emission. In addition, the background Galactic and extragalactic diffuse emission were added in the source model using the spectral model `gll_iem_v06.fits` and file `iso_P8R2_SOURCE_V6_v06.txt` respectively. The normalizations of the diffuse components were free parameters in the analysis.

### 2.2. Source Search in Whole Data

Using the LAT science tools software package `v11r5p3`, we first performed standard binned likelihood analysis to the LAT data for GRO J1008–57. Since below 300 MeV, the instrument response function of the LAT has relatively large uncertainties and Galactic background emission is also strong, we chose events above 300 MeV for the likelihood analysis. The obtained Test Statistic (TS) value at the position of GRO J1008–57 was  $\simeq 11$ . The TS value at a position indicates the fit improvement for including a source, and is approximately the square of the detection significance of the source (Abdo et al. 2010). Therefore we found possible detection with  $>3\sigma$  significance.

We checked whether the  $\gamma$ -ray emission was due to contamination by nearby sources which were not included in the *Fermi* LAT 4-year catalog. A preliminary LAT 8-year point source list was released in early 2018, which contains nearly 2500 new sources, although it is not encouraged to use this list directly<sup>2</sup>. In addition, the extended source templates and the Galactic and extragalactic diffuse emission models have not been updated accordingly. We thus only added nearby new sources to the source model, and re-performed the maximum likelihood analysis. In this analysis, we only found  $TS \simeq 7$  at the position of GRO J1008–57, which is low for a possible detection.

### 2.3. Orbital-phase Resolved Search

Because Be XRBs often show enhanced emission at certain orbital phase ranges, particularly indicated by those  $\gamma$ -ray binaries, we searched for possible  $\gamma$ -ray emission in 10 orbital phase ranges of GRO J1008–57 (i.e., 0.0–0.1, ..., 0.9–1.0, with phase zero at the periastron). Likelihood analysis to the data in each of the phase bins was performed. We found during phase 0.8–0.9 and 0.5–0.7 (defined as Phase I and II, respectively), the source was possibly detected with  $TS > 9$ . In Figure 1, its 0.3–500 GeV orbital light curve and TS curve in 10 orbital-phase bins are shown. For the data points not in Phase I and II, their TS values were smaller than 5 ( $<2\sigma$  significance), and the 95% (at  $2\sigma$  level) flux upper limits were derived.

#### 2.3.1. Phase I

The  $\gamma$ -ray emission was significantly detected with a TS value of  $\sim 20$ . Photon index  $\Gamma = 2.2 \pm 0.2$  and 0.3–500

<sup>2</sup> <https://fermi.gsfc.nasa.gov/ssc/data/access/lat/fl8y/>

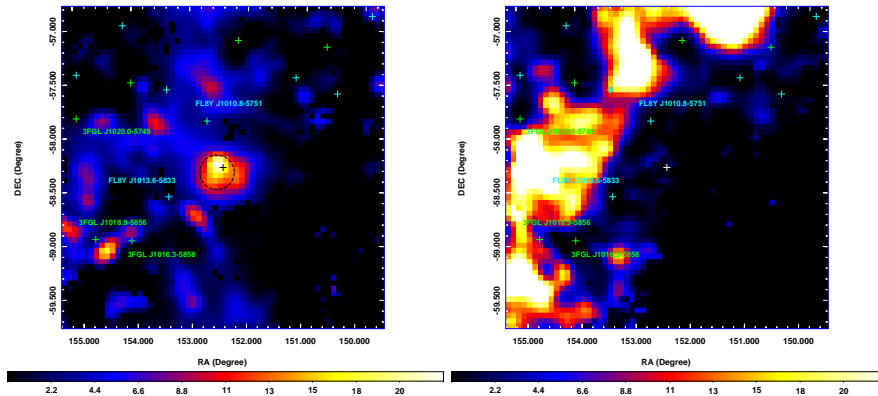


FIG. 2.— Residual TS maps for GRO J1008-57, with a size of  $3^\circ \times 3^\circ$ , in 0.5–39 GeV band during Phase I (left) and the phase ranges excluding Phase I (right). All sources in the source model were considered and removed. The image scale of the maps is  $0^\circ 05 \text{ pixel}^{-1}$ , with the color bar indicating the TS value range. The green and light blue pluses mark the positions of the catalog sources listed in the 4-year and 8-year *Fermi* LAT source catalogs, respectively. The black (or white) plus and black circle mark the position of GRO J1008-57 and the  $2\sigma$  error circle of the best-fit position, respectively.

TABLE 1  
*Fermi* LAT FLUX MEASUREMENTS OF GRO J1008-57

$E$ (GeV)	Band (GeV)	Phase I		Phase II	
		$F/10^{-12}$ ( $\text{erg cm}^{-2} \text{ s}^{-1}$ )	TS	$F/10^{-12}$ ( $\text{erg cm}^{-2} \text{ s}^{-1}$ )	TS
0.15	0.1–0.2	9.1	0	6.8	0
0.36	0.2–0.5	5.2	0	3.5	0
0.84	0.5–1.3	$6 \pm 3$	9	1.1	0
1.97	1.3–3.0	5.1	0	2.2	0
4.62	3.0–7.1	$2 \pm 1$	6	2.4	2
10.83	7.1–16.6	4	1	2.0	1
25.37	16.6–38.8	$3 \pm 1$	7	$3 \pm 1$	10
59.46	38.8–91.0	5.2	0	3.1	0
139.36	91.0–213.3	10.8	0	5.3	0
326.60	213.3–500.0	22.2	0	30.8	2

Note:  $F$  is the energy flux ( $E^2 dN/dE$ ). Fluxes without uncertainties are 95% upper limits.

GeV flux  $F_{0.3-500} = 13 \pm 4 \times 10^{-12} \text{ erg s}^{-1} \text{ cm}^{-2}$  were obtained during Phase I from the maximum likelihood analysis. We extracted the  $\gamma$ -ray spectrum by performing maximum likelihood analysis of the LAT data in 10 evenly divided energy bands in logarithm from 0.1–500 GeV. In the extraction, the spectral normalizations of the sources within 5 degrees from GRO J1008-57 were set as free parameters, while the other parameters of the sources were fixed at the values obtained from the above maximum likelihood analysis. A point source with power-law emission was assumed for GRO J1008-57, and the  $\Gamma$  value was fixed to 2. We kept only spectral data points with the flux values 2 times greater than the uncertainties, and otherwise derived 95% (at  $2\sigma$  level) flux upper limits. The obtained flux and TS values of the spectral data points are given in Table 1.

We also calculated the residual TS map during Phase I in the energy range of 0.5–39 GeV. This energy range covers the three spectral data points with  $\text{TS} > 4$  (Table 1). The TS map is shown in the left panel of Figure 2. There is  $\gamma$ -ray emission present at the position of GRO J1008-57 with a TS of  $\sim 22$ . We ran *gtfindsrc* to determine the position of the  $\gamma$ -ray emission, and obtained R.A.=152°5, Decl.=−58°3, (equinox J2000.0), with  $1\sigma$  nominal uncertainty of  $0^\circ 1$ . GRO J1008-57 is  $0^\circ 07$  from this position and within the  $1\sigma$  error circle,

indicating the likely association. As a comparison, the 0.5–39 GeV TS map excluding the data in Phase I was also calculated (shown in the right panel of Figure 2). No  $\gamma$ -ray emission is present as  $\text{TS} \sim 0$  at the position of GRO J1008-57. The comparison of the two TS maps support the detection of GRO J1008-57 in Phase I.

### 2.3.2. Phase II

There are also marginal detections with  $>2\sigma$  significance during phase 0.5–0.7. We searched for possible detection during this wide phase range, and found that the  $\gamma$ -ray emission can be detected with a TS of 10 ( $>3\sigma$  significance).  $\Gamma = 1.5 \pm 0.3$  and  $F_{0.3-500} = 9 \pm 7 \times 10^{-12} \text{ erg s}^{-1} \text{ cm}^{-2}$  were obtained from the maximum likelihood analysis. We extracted the  $\gamma$ -ray spectrum during Phase II, and the obtained flux and TS values of the spectral data points are provided in Table 1. There is actually only one spectral data point possibly detected,  $\text{TS} \sim 10$  in energy band of 16.6–38.8 GeV. Comparing to the results obtained in Phase I,  $\Gamma$  is lower in Phase II, although the uncertainties are too large for drawing a conclusion.

We calculated the residual TS map in 16.6–38.8 GeV band during Phase II, which is shown in the middle panel of Figure 3. The TS maps in this energy band during Phase I and the remaining phase ranges were also calculated, which are shown in the left and right panel of Figure 3 respectively. While the residual at the position of GRO J1008-57 in Phase II has  $\text{TS} \sim 10$ , the map is noisy with other residuals. The situation is worse in Phase I, as a residual with  $\text{TS} \sim 9$  is slightly off the position of GRO J1008-57 and there are several other residuals with similar TS values. In the remaining phase ranges,  $\text{TS} \sim 0$  at the source position. The TS maps suggest that given the narrow energy range used, we may see marginal evidence for the detection of GRO J1008-57 in Phase II, but no clear conclusion can be made.

### 2.3.3. Possible Emission Contamination

GRO J1008-57 is located in a complex region with a few sources detected relatively nearby and the  $\gamma$ -ray emission could only be detected during some phase ranges. We thus checked whether the nearby catalog

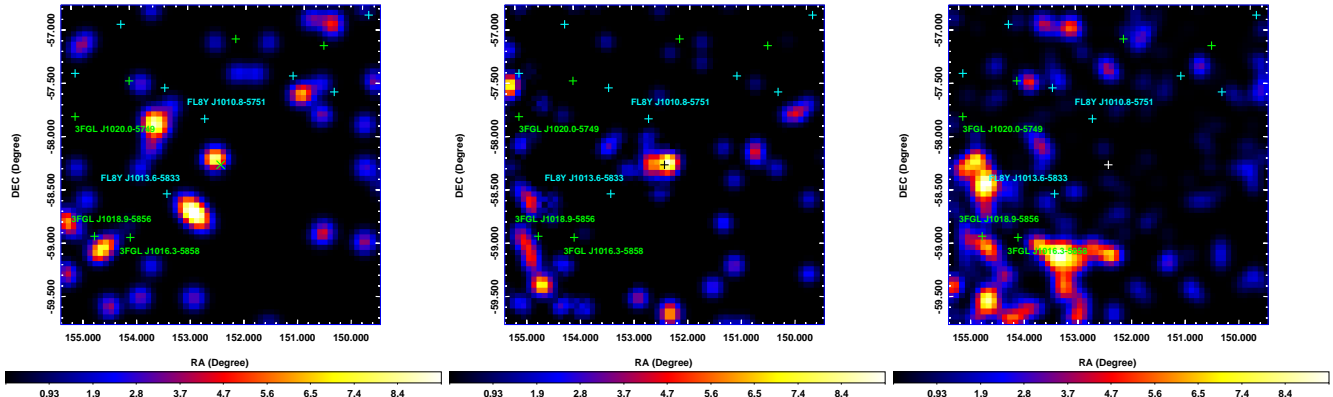


FIG. 3.— Residual TS maps for GRO J1008–57, with a size of  $3^\circ \times 3^\circ$ , in 16.6–38.8 GeV band during Phase I, II, and the remaining phase ranges (*left*, *middle*, and *right*, respectively). All sources in the source model (from the 4-year and 8-year Fermi LAT source catalogs) were considered and removed (marked with green and light blue pluses, respectively). The image scale of the maps is  $0.05 \text{ pixel}^{-1}$ , with the color bar indicating the TS value range. The position of GRO J1008–57 is in the center of the maps, marked with green cross in the *left* panel and black or white plus in the other two panels.

sources are variable, whose flux variations might affect our results. There are six nearby sources listed in the LAT 4-year catalog (see Figure 2). The brightest one (3FGL J1018.9–5856) is a  $\gamma$ -ray binary, two of them (3FGL J1016.3–5858 and 3FGL J1020.0–5749) are  $\gamma$ -ray pulsars (PSR J1016–5857 and PSR J1019–5749, respectively), and the other three are unidentified sources. We first checked the 0.1–300 GeV variability indices (Acero et al. 2015) of them, and found none of them has variability index greater than the threshold to be identified as a variable source. There are also eight new sources listed in the LAT 8-year point source catalog (see Figure 2). For them, we calculated the 0.3–500 GeV variability indices for two of them (FL8Y J1010.8–5751 and FL8Y J1013.6–5833, the two closest to GRO J1008–57) following the method used in Acero et al. (2015). Both of these two sources are unidentified sources, and have variability indices (80.3 for J1010.8–5751 and 82.4 for J1013.6–5833) smaller than the threshold (149.7 for 112 degrees of freedom) considered for a variable source. We then checked the 0.3–500 GeV fluxes of these nearby sources during the 10 orbital phase bins of GRO J1008–57. For each of the sources, the fluxes during each bins have  $<2\sigma$  deviations from those derived from the likelihood analysis of the whole data, again indicating no significant variations. We also checked the SIMBAD Astronomical Database and found that except GRO J1008–57, there are only a few normal stars known within the  $2\sigma$  error circles of the position obtained during Phase I. Therefore no evidence was found to indicate any possible emission contamination from nearby sources.

### 3. DISCUSSION

Having analyzed nine years of the Fermi LAT Pass 8 data, we searched for  $\gamma$ -ray emission from Be X-ray binaries with known orbital parameters. The search was conducted in the whole data and orbital-phase resolved data. Only for GRO J1008–57, possible residual emission was found in the whole data, but without sufficiently high significance. In the orbital-phase resolved analysis, the GRO J1008–57 region was found to have excess  $\gamma$ -ray emission significantly detected during the orbital phase

TABLE 2  
THREE TS>9 DETECTIONS IN 0.1 ORBITAL PHASE BINS

Central Time (MJD)	Orbital Phase	TS
55135.728	0.8–0.9	9.7
55559.844	0.5–0.6	9.1
56383.128	0.8–0.9	17.5

range of 0.8–0.9 and possibly also at 0.5–0.7. The  $\gamma$ -ray emission may be described with a power law with  $\Gamma \sim 2$ , although the spectra suffer large uncertainties. The likely orbital dependence of the excess  $\gamma$ -ray emission supports its association with GRO J1008–57.

Since GRO J1008–57 is considered as a transient X-ray pulsar, with pulsed X-ray emission detected during the outbursts, accretion onto the neutron star certainly occurs at least in outbursts. No mechanisms or related physical processes are known to be able to produce  $\gamma$ -ray emission during neutron star’s active accretion. The likely detection of GRO J1008–57 in phase 0.8–0.9, not during the periastron passage, is consistent with this fact. When in quiescence, the X-ray luminosity of GRO J1008–57 is generally  $>10^{34} \text{ erg s}^{-1}$ , and in one *Swift* monitoring of the binary over a full orbital cycle, the luminosity stayed at a level of  $\sim 10^{35} \text{ erg s}^{-1}$ , higher than that for the onset of the propeller phase (Tsygankov et al. 2017). It is thus likely that there is always sufficiently strong mass accretion in the accretion disk surrounding the neutron star, not allowing a possible switch for the neutron star from being accretion powered to rotation powered (such as in the accretion-powered millisecond pulsar binary SAX J1808.4–3658; see, e.g., Burderi et al. 2003; Wang et al. 2013). The scenario for the  $\gamma$ -ray production from PSR B125963/LS 2883 does not work for GRO J1008–57.

In addition to neutron star  $\gamma$ -ray binaries, another small group of so-called transitional millisecond pulsar (MSP) binary systems, with PSR J1023+0038 as a prototype (Archibald et al. 2009), are also known to produce much enhanced  $\gamma$ -ray emission during their active state when an accretion disk is present around the pulsar (Wang et al. 2009; Stappers et al. 2014; Takata et al. 2014). These systems switch between the active state

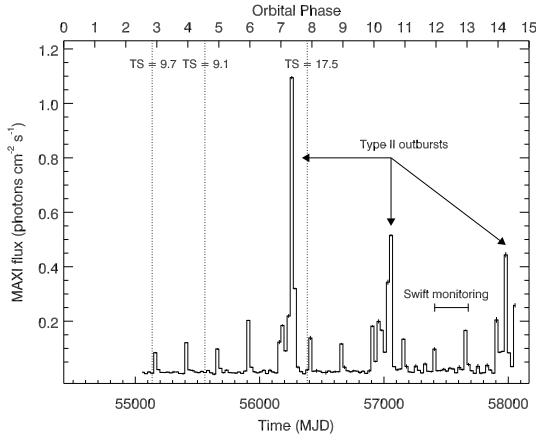


FIG. 4.— *Fermi* LAT detections of GRO J1008–57 in three 0.1 orbital phases. The *MAXI* (Matsuoka et al. 2009) X-ray light curve of GRO J1008–57 is plotted to show the outburst events. The occurrences of the three detections are marked with dotted lines. The full orbital cycle observed with *Swift* (Tsygankov et al. 2017) is also marked.

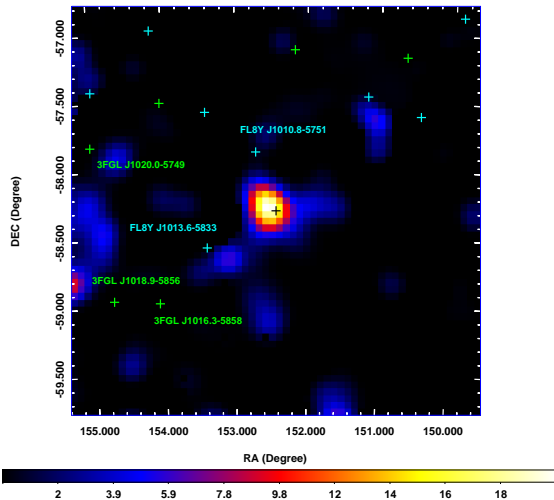


FIG. 5.— TS map of the GRO J1008–57 region during the single orbital phase 0.8–0.9 right after the 2012 November type-II outburst. Excess emission with  $TS=17.5$  is clearly seen at the position of GRO J1008–57 (marked with a black plus). All sources in the source model (from the 4-year and 8-year *Fermi* LAT source catalogs) were considered and removed (marked with green and light blue pluses, respectively). The image scale of the maps is  $0.05 \text{ pixel}^{-1}$ , with the color bar indicating the TS value range.

and disk-free state, and in the latter they are more like a typical MSP binary and do not have an accretion disk. Although the radiation mechanism for the enhanced  $\gamma$ -ray emission in the active state is not certain, the scenarios of an active (or partially active; see Xing et al. 2018) radio pulsar interacting the accretion disk (Takata et al. 2014) or a propelling neutron star (Papitto et al. 2014; Papitto & Torres 2015) have been proposed. Possible evidence for the former scenario is the coherent X-ray and optical pulsations detected in emission from PSR J1023+0038 in the active state (Archibald et al. 2015; Ambrosino et al. 2017; note no radio pulsations are seen). These features indicate that very complicated processes can occur in a seemingly accreting pulsar.

The corotation radius  $r_c$  of PSR J1023+0038 is small,  $r_c \simeq 1.7 \times 10^8 M_{1.4}^{1/3} P^{2/3} \text{ cm} \simeq 2.4 \times 10^6 \text{ cm}$ , where  $M_{1.4}$  is the neutron star mass in units of  $1.4 M_\odot$ , and its magnetospheric radius  $r_m$  can be estimated to be of the order of  $10^7 \text{ cm}$  (Papitto & Torres 2015). On the basis of the accretion scenario for neutron stars generally considered (Frank et al. 2002), PSR J1023+0038 is in the propeller phase in the active state, as  $r_m > r_c$  (the inner edge of the disk does not reach the corotation radius). For GRO J1008–57, its  $r_c \simeq 3.5 \times 10^9 \text{ cm}$  and  $r_m \simeq 5.7 \times 10^8 M_{1.4}^{1/7} R_6^{-2/7} L_{35}^{-2/7} \mu_{30}^{4/7} \simeq 1.9 \times 10^9 L_{35}^{-2/7} \text{ cm}$ , where the neutron star radius  $R_6$  is in units of  $10^6 \text{ cm}$ ,  $L_{35}$  is the X-ray luminosity in units of  $10^{35} \text{ erg s}^{-1}$ , and  $\mu_{30}$  is the magnetic moment in units of  $10^{30} \text{ G cm}^3$  ( $\mu_{30} = 8$  assumed for GRO J1008–57). Because  $r_m$  is slightly smaller than  $r_c$ , GRO J1008–57 would switch to be in the propeller phase once its  $L$  is lower than  $10^{34} \text{ erg s}^{-1}$  (see also Tsygankov et al. 2017), opening the possibility to be in the  $\gamma$ -ray emitting scenarios suggested by Papitto & Torres (2015) or Takata et al. (2014).

Following this idea, we further performed the likelihood analysis to the LAT data in each time intervals of 0.1 orbital phase of GRO J1008–57 (i.e., 24.9 days). We found that there were three detections with  $TS > 9$ , which are listed in Table 2. Two detections were in phase 0.8–0.9 and one in 0.5–0.6, and their occurrences are shown in Figure 4, comparing to the X-ray outburst activity. It can be seen that the detection with the highest TS value (17.5) was in the phase of 0.8–0.9, right after a bright type-II outburst (occurred in November 2012 at an orbital phase of  $\sim 0.3$ ) during the same orbital cycle. The TS map for this detection was calculated and is shown in Figure 5, indicating clear excess emission at the position of GRO J1008–57. A fine light curve (5 day binned) during this orbital phase was constructed, but no clear pattern, such as a flaring event, could be identified (which actually excludes possibilities of contamination by a Solar flare or a  $\gamma$ -ray burst; both would appear as bright and sharp flaring events in daily LAT light curves).

Given the detections, particularly the highest TS one, we thus suggest that the combination of the stellar rotation, magnetic field, and mass accretion for the neutron star in GRO J1008–57 makes it a unique system, which occasionally switches to be in a propeller phase when the accretion rate is low (indicated by  $L \lesssim 10^{34} \text{ erg s}^{-1}$ ). During the phase, either the propelling processes or a partially active radio pulsar (similar to PSR J1023+0038) give rise to  $\gamma$ -ray emission. The detections in our orbital-phase resolved analysis are due to the adding up of the occasional emission from the system. Such an event occurred after the giant type-II outburst in November 2012. Matter in the accretion disk might be used up in the outburst, allowing the system to have a switch in the following orbital phase during the same cycle. Unfortunately high-sensitivity X-ray observations at the time only targeted at the outburst (Kühnel et al. 2017); otherwise X-ray observations would be able to provide evidence by detecting low-luminosity emission from the source. We note that during the orbital cycle of having  $\sim 10^{35} \text{ erg s}^{-1}$  X-ray luminosity, monitored with *Swift* (see Figure 4), no  $\gamma$ -ray detection was found. This fact might be indirect evidence supporting our sug-

gestion.

In order to investigate this possibility, close X-ray monitoring after a giant type-II outburst should be conducted. Combining with *Fermi* LAT monitoring, evidence of a low X-ray luminosity state plus simultaneous detection of  $\gamma$ -ray emission may be found. If this possibility is confirmed from such joint observations, GRO J1008–57 would represent a type of transient  $\gamma$ -ray emitting neutron-star XRBs. When the neutron star is in a propeller phase, due to some material ejection processes or interaction of a (partial pulsar) wind with surrounding material, the XRB would also emit  $\gamma$ -rays.

## REFERENCES

- Abdo, A. A., Ackermann, M., Ajello, M., et al. 2009, *ApJ*, 701, L123  
 —. 2010, *ApJS*, 188, 405  
 —. 2011, *ApJ*, 736, L11  
 Acciari, V. A., Aliu, E., Araya, M., et al. 2011, *ApJ*, 733, 96  
 Acero, F., Ackermann, M., Ajello, M., et al. 2015, *ApJS*, 218, 23  
 Aharonian, F., Akhperjanian, A. G., Anton, G., et al. 2009, *A&A*, 507, 389  
 Ambrosino, F., Papitto, A., Stella, L., et al. 2017, *Nature Astronomy*, 1, 854  
 Archibald, A. M., Stairs, I. H., Ransom, S. M., et al. 2009, *Science*, 324, 1411  
 Archibald, A. M., Bogdanov, S., Patruno, A., et al. 2015, *ApJ*, 807, 62  
 Atwood, W. B., Abdo, A. A., Ackermann, M., et al. 2009, *ApJ*, 697, 1071  
 Bongiorno, S. D., Falcone, A. D., Stroh, M., et al. 2011, *ApJ*, 737, L11  
 Burderi, L., Di Salvo, T., D’Antona, F., et al. 2003, *Chinese Journal of Astronomy and Astrophysics Supplement*, 3, 311  
 Cheng, K. S., & Ruderman, M. 1991, *ApJ*, 373, 187  
 Chernyakova, M., Abdo, A. A., Neronov, A., et al. 2014, *MNRAS*, 439, 432  
 Coe, M. J., Bird, A. J., Hill, A. B., et al. 2007, *MNRAS*, 378, 1427  
 Davidson, K., & Ostriker, J. P. 1973, *ApJ*, 179, 585  
 Dubus, G. 2013, *A&A Rev.*, 21, 64  
 Frank, J., King, A., & Raine, D. J. 2002, *Accretion Power in Astrophysics: Third Edition*, 398  
 Hadasch, D., Torres, D. F., Tanaka, T., et al. 2012, *ApJ*, 749, 54  
 Hinton, J. A., Skilton, J. L., Funk, S., et al. 2009, *ApJ*, 690, L101  
 Ho, W. C. G., Ng, C.-Y., Lyne, A. G., et al. 2017, *MNRAS*, 464, 1211  
 Johnston, S., Manchester, R. N., Lyne, A. G., et al. 1992, *ApJ*, 387, L37  
 Johnston, S., Manchester, R. N., Lyne, A. G., Nicastro, L., & Spyromilio, J. 1994, *MNRAS*, 268, 430  
 Kühnel, M., Müller, S., Kreykenbohm, I., et al. 2013, *A&A*, 555, A95  
 Kühnel, M., Fürst, F., Pottschmidt, K., et al. 2017, *A&A*, 607, A88  
 Lamers, H. J. G. L. M., van den Heuvel, E. P. J., & Petterson, J. A. 1976, *A&A*, 49, 327  
 Li, J., Torres, D. F., Cheng, K.-S., et al. 2017, *ApJ*, 846, 169  
 Liu, Q. Z., van Paradijs, J., & van den Heuvel, E. P. J. 2006, *VizieR Online Data Catalog*, 345  
 Lutovinov, A. A., & Tsygankov, S. S. 2009, *Astronomy Letters*, 35, 433  
 Lyne, A. G., Stappers, B. W., Keith, M. J., et al. 2015, *MNRAS*, 451, 581  
 Matsuoka, M., Kawasaki, K., Ueno, S., et al. 2009, *PASJ*, 61, 999  
 Meurs, E. J. A., & van den Heuvel, E. P. J. 1989, *A&A*, 226, 88  
 Papitto, A., & Torres, D. F. 2015, *ApJ*, 807, 33  
 Papitto, A., Torres, D. F., & Li, J. 2014, *MNRAS*, 438, 2105  
 Reig, P. 2011, *Ap&SS*, 332, 1  
 Romero, G. E., Kaufman Bernadó, M. M., Combi, J. A., & Torres, D. F. 2001, *A&A*, 376, 599  
 Shrader, C. R., Sutaria, F. K., Singh, K. P., & Macomb, D. J. 1999, *ApJ*, 512, 920  
 Stappers, B. W., Archibald, A. M., Hessels, J. W. T., et al. 2014, *ApJ*, 790, 39  
 Stollberg, M. T., Finger, M. H., Wilson, R. B., et al. 1993, *IAU Circ.*, 5836  
 Takata, J., Li, K. L., Leung, G. C. K., et al. 2014, *ApJ*, 785, 131  
 Tam, P. H. T., Huang, R. H. H., Takata, J., et al. 2011, *ApJ*, 736, L10  
 Tam, P. H. T., Li, K. L., Takata, J., et al. 2015, *ApJ*, 798, L26  
 Tsygankov, S. S., Wijnands, R., Lutovinov, A. A., Degenaar, N., & Poutanen, J. 2017, *MNRAS*, 470, 126  
 Walter, R., Lutovinov, A. A., Bozzo, E., & Tsygankov, S. S. 2015, *A&A Rev.*, 23, 2  
 Wang, Z., Archibald, A. M., Thorstensen, J. R., et al. 2009, *ApJ*, 703, 2017  
 Wang, Z., Breton, R. P., Heinke, C. O., Deloye, C. J., & Zhong, J. 2013, *ApJ*, 765, 151  
 Xing, Y., Wang, Z., & Takata, J. 2016, *ApJ*, 828, 61  
 Xing, Y., Wang, Z.-X., & Takata, J. 2018, *Research in Astronomy and Astrophysics*, 18, 127